Commun. Comput. Phys.
doi: 10.4208/cicp.2009.09.026

Vol. 7, No. 4, pp. 759-778
April 2010

# Image Selective Segmentation under Geometrical Constraints Using an Active Contour Approach

Noor Badshah and Ke Chen*

*Centre for Mathematical Imaging Techniques (CMIT), Department of Mathematical Sciences, The University of Liverpool, Liverpool L69 7ZL, United Kingdom.*

Received 3 February 2009; Accepted (in revised version) 10 September 2009

Available online 3 November 2009

**Abstract.** In this paper we propose a new model for segmentation of an image under some geometrical constraints in order to detect special regions of interest. Our work is based on the recent work by Gout et al. [Numer. Algorithms, 39 (2005), pp. 155-173 and 48 (2008), pp. 105-133] using geodesic active contours models, by combining it with the idea of a piecewise constant Mumford-Shah model as with the non-selective Chan-Vese segmentation. Numerical tests show that our method is more robust than the previous works.

**AMS subject classifications**: 62H35, 65N22, 65N55, 74G65, 74G75

**Key words**: Active contours, energy minimization, partial differential equations, segmentation, level sets, geometric constraints.

## 1 Introduction

An important problem in image processing is the segmentation of a picture representing a real scene, into classes or categories, corresponding to different objects and the background in the image. In the end, each pixel should belong to one class and only one. In other words, we look for a partition of the image into distinct segments each having some features in common, e.g., intensities, colour or texture. A variety of different techniques have been developed to solve the problem of image segmentation, such as region growing and emerging [1], watershed algorithms [31], minimum description length criteria [21], and Mumford-Shah energy minimization [22]. Recently, PDE-based active contour models [20, 29] for curve evolution have been popular for image segmentation. In our recent work [4–6], we have developed effective multilevel algorithms for the Chan-Vese [14] approach for implementing active contours without edges. In [7,11] the authors discussed the global minimizers of the snake models.

*Corresponding author. *Email addresses:* noor.badshah@liv.ac.uk (N. Badshah), k.chen@liv.ac.uk (K. Chen)

 

While the above segmentation models are useful for various applications, however, other imaging problems require the functionality of selectivity, i.e., only segment a particular part among those objects that have the same feature. Such situations are ubiquitous in medical imaging especially in CT images where most objects (organs) have similar intensities. For example, we might like to segment the left kidney only whilst the above methods will give both kidneys mixed other organs. For the simple example in Fig. 3, it is fairly easy to segment the image to obtain 4 objects together but not separately because these four objects belong to the same intensities-based class. The task of a selective segmentation is how to detect only one of them, given additional information. Following Gout et al. [18], we consider the case of geometric constraints in terms of a list of given points near the interested objects to aid segmentation.

We remark that geometric constraints are also necessary for normal segmentation methods whenever the interface between objects is not 'clearly' visible due to poor image quality or some occultation. Curve evolution means to evolve deformable contours subject to constraints towards the boundary of the object to be detected. This deformation is made trying to minimize a functional depending on the curve and defined so that a local minimum is obtained at the boundary of the object. Casselles et al. [8] have shown, for example, that setting one of the regularization parameters to zero in the classical active contour model is equivalent to finding a geodesic curve in a Riemann space whose metric depends on the image content [18], because an edge in an image is the locus of points for which the image gradient rapidly varies. However when data acquisition cannot be performed in an ideal manner, this criterion can no longer be applied. This is the case when two objects, having similar homogeneous intensity or texture etc, are very close to each other. Then it is hard to clearly identify the interface without additional information. Here we consider geometrical constraints consisting of a set of points belonging to the contour of interest. For a medical image, practically, the expert needs to click on the organ under consideration a couple of times.

To proceed, let $z(x,y)$ be the given image defined on a rectangular domain $\Omega$. The geometrical constraints in terms of a set of $n_1$ points near the boundary of object to be detected are defined by $A=\{(x_i,y_i)\in\Omega,\ 1\leq i\leq n_1\}\subset\Omega$. The aim is to find an optimal contour $\Gamma\subset\Omega$ that best approaches the points from the set $A$ while detecting the desire object in an image.

Recently Gout et al. [18] proposed a model based on geodesic active contours for solving this problem. Their model uses image gradient information $|\nabla z|$, to stop the contour evolution. If the given image $z$ is very noisy, then the isotropic smoothing Gaussian has to be used, which will smooth the edges in an undesirable manner. While this model can detect objects correctly for many examples, we found that it is sensitive to parameter choice and hence it can fail to work for some images. Here to increase robustness, we modify their model by combining it with the idea from Chan-Vese model [14], which helps in segmenting noisy images without an isotropic smoothing Gaussian and also helps to segment images with fuzzy boundaries, as verified later.

This paper is organized in the following way. Section 2 contains a review of the ex-

isting model of Gout et al. [18]. In Section 3 we present our proposed new model of minimization and derive the Euler-Lagrange equation. In Section 4 we describe a semi-implicit method and an additive operator splitting (AOS) method for solving the PDE. In Section 5 we give some experimental results.

## 2 An image segmentation model using geodesic active contours and geometrical constraints (M-1)

The model by Gout et al. [18] builds the given geometrical constraints into a geodesic active contour model [8]. The constraints will be represented by a distance function $d(x,y)$ (which is towards zero when near the given points and is towards one elsewhere) and the geodesic model requires an edge detector function $g$ (which is zero on edges and is one at homogenous regions).

In [18] the following edge detector function, a popular choice [8,13], is used

$$g(w)=\frac{1}{1+w^2}.$$

Clearly $g(|\nabla z(x,y)|)$ is zero on edges in an image and is 1 in flat regions. The purpose of the edge detector function $g$ is to stop the evolving curve on edges of the objects. To stop the evolving curve going away from the points from set $A$, the following distance function $d$ is defined in [18]:

$$d(x,y)=\prod_{i=1}^{n_1}\left(1-e^{-\frac{(x-x_i)^2}{2\sigma^2}}e^{-\frac{(y-y_i)^2}{2\sigma^2}}\right),\quad \forall(x,y)\in\Omega. \tag{2.1}$$

Another option for $d$ is

$$d(x,y)=distance((x,y),A)=\frac{\min_{(x_i,y_i)\in A}\left|(x,y)-(x_i,y_i)\right|}{M}$$

for all $(x,y)\in\Omega$ and $i=1,2,\cdots,n_1$ used in [17]; here we added the scaling factor $M=\max_{(x_i,y_i)\in A,(x_a,y_a)\in\Omega}|(x_a,y_a)-(x_i,y_i)|$ to ensure $0\le d\le 1$. Here we mainly use (2.1). Clearly $d$ acts locally and will be approximately 0 in the neighborhood of points of $A$. The aim of their model is to find a contour $\Gamma$ such that $g\simeq 0$ in the vicinity of $d\simeq 0$, by minimizing the following energy

$$F(\Gamma)=\int_\Gamma dg(|\nabla z|)ds. \tag{2.2}$$

Here the contour $\Gamma$ will stop where $g\simeq 0$ (near object boundaries) in the neighborhood of points for $A$ where $d\simeq 0$.

**Level Set Formulation of the Model**. To extend the domain of the integral in (2.2) to the whole image other than $\Gamma$, the level set approach [25, 26, 28] is the best option. Let $\phi:\Omega\to\mathbb{R}$ be a Lipschitz continuous function whose zero level set is $\Gamma$, i.e.,

$$\Gamma=\{(x,y)\in\Omega:\phi(x,y)=0\},$$

with $\phi<0$ inside $\Gamma$ and $\phi>0$ outside $\Gamma$. In terms of the level set formulation, equation (2.2) becomes

$$F(\phi)=\int_\Omega d(x,y)g(|\nabla z(x,y)|)|\nabla H(\phi(x,y))|dxdy,$$

where $H$ is the one-dimensional Heaviside function and $\int_\Omega|\nabla H(\phi(x,y))|dxdy$ is the length of $\Gamma$. Thus we have the following minimization problem

$$\min_{\phi(x,y)} F(\phi(x,y)).$$

Since the Heaviside function is not differentiable at the origin, we consider the regularized version of $H$ denoted by $H_\epsilon$ and is given by [14, 15, 25]:

$$H_\epsilon(x)=\frac{1}{2}\Big(1+\frac{2}{\pi}\arctan(\frac{x}{\epsilon})\Big),\quad \delta_\epsilon(x)=H_\epsilon'(z)=\frac{1}{\pi}\frac{\epsilon}{\epsilon^2+x^2}. \tag{2.3}$$

Thus the minimization problem becomes

$$\min_{\phi(x,y)} F_\epsilon(\phi(x,y)), \tag{2.4}$$

where

$$F_\epsilon(\phi(x,y))=\int_\Omega d(x,y)g(|\nabla z(x,y)|)\delta_\epsilon(\phi)|\nabla\phi(x,y)|dxdy. \tag{2.5}$$

Minimization with respect to $\phi(x,y)$ leads to the following Euler-Lagrange equation

$$-\delta_\epsilon(\phi(x,y))\nabla\cdot\left(d(x,y)g(|\nabla z(x,y)|)\frac{\nabla\phi(x,y)}{|\nabla\phi(x,y)|}\right)=0.$$

Gout et al [18] considered the following equation with artificial time step $t$:

$$\frac{\partial\phi(x,y,t)}{\partial t}=\delta_\epsilon(\phi(x,y,t))\nabla\cdot\left(d(x,y)g(|\nabla z(x,y)|)\frac{\nabla\phi(x,y,t)}{|\nabla\phi(x,y,t)|}\right) \tag{2.6}$$

with the boundary condition

$$\frac{\delta_\epsilon(\phi(x,y,t))}{|\nabla\phi(x,y,t)|}\frac{\partial\phi(x,y,t)}{\partial\vec{n}}=0,$$

where $\vec{n}$ is the outward unit normal to the boundary $\partial\Omega$. Clearly the quantity $\frac{\partial\phi(x,y,t)}{\partial t}$ tends to 0 when a local minimum is achieved. In other words if the model converges and the curve will not evolve any more since a steady state has been reached. Replacing $\delta_\epsilon(\phi(x,y,t))$ by $|\nabla\phi(x,y,t)|$, a motion is applied to all level sets and it makes the flow independent of the scaling of $\phi$ [2,34]; more details can be found in [17,18]. The following evolution problem was considered

$$\begin{aligned}&\frac{\partial\phi(x,y,t)}{\partial t}=|\nabla\phi(x,y,t)|\nabla\cdot\left(d(x,y)g(|\nabla z(x,y)|)\frac{\nabla\phi(x,y,t)}{|\nabla\phi(x,y,t)|}\right),\\&\frac{\partial\phi(x,y,t)}{\partial\vec{n}}=0\quad\text{ on }\partial\Omega,\end{aligned}\tag{2.7}$$

with $\phi(x,y,0)=\phi_0(x,y)$, where $\phi_0(x,y)$ is the initial value of the desirable $\phi(x,y)$. To speed the convergence of the model they added an extra term $\alpha d(x,y)g(|\nabla z(x,y)|)$ known as a "balloon term" [16] to the evolution equation of a level set, where $\alpha$ is any constant. This term prevents the curve from stopping on a non significant local minimum and is also of importance when initializing the process with a curve inside the object to be detected. Thus the evolution problem becomes

$$\begin{aligned}\frac{\partial\phi(x,y,t)}{\partial t}&=|\nabla\phi(x,y,t)|\nabla\cdot\left(d(x,y)g(|\nabla z(x,y)|)\frac{\nabla\phi(x,y,t)}{|\nabla\phi(x,y,t)|}\right)\\&\quad+\alpha d(x,y)g(|\nabla z(x,y)|)|\nabla\phi(x,y,t)|,\\\frac{\partial\phi(x,y,t)}{\partial n}&=0\quad\text{ on }\partial\Omega,\end{aligned}$$

with $\phi(x,y,0)=\phi_0(x,y)$. The above equation can be written as

$$\begin{aligned}\frac{\partial\phi(x,y,t)}{\partial t}&=|\nabla\phi(x,y,t)|d(x,y)g(|\nabla z(x,y)|)\nabla\cdot\left(\frac{\nabla\phi(x,y,t)}{|\nabla\phi(x,y,t)|}\right)\\&\quad+\nabla(d(x,y)g(|\nabla z(x,y)|))\cdot\nabla\phi\\&\quad+\alpha d(x,y)g(|\nabla z(x,y)|)|\nabla\phi(x,y,t)|.\end{aligned}\tag{2.8}$$

Further an AOS method [23,32] was used to solve (2.8).

We remark that this model is based on geodesic active contours in which an edge detector plays a major role. However such detectors use only local information of the boundary (gradient and curvature information) to detect the boundary itself which inevitably runs into difficulties when dealing with fuzzy edges and discrete edges. Furthermore because of the local attributes and the dependence on gradients, geodesic active contours are heavily affected by noisy inputs; it is hard to detect objects from a noisy image. One can use isotropic Gaussian smoothing, but this will smooth the edges too. Below we propose a new model where an added stopping term is based on Mumford and Shah segmentation techniques [14,22]. With this new model we can detect objects in noisy images without using isotropic Gaussian smoothing.

## 3 A modified selective segmentation model (M-2)

The Chan-Vese (CV) model [14] is a special case of the piecewise constant Mumford and Shah model [22] when restricted to only 2 phases. The CV model is not based on the gradient of the image $z(x,y)$ for the stopping process. It can detect contours both with and without gradients. Also there is no need to smooth the image in the case of a noisy image. To take the advantages of the CV model [14] for selective segmentation, we add $\lambda_1\int_{inside(\Gamma)}|z(x,y)-c_1|^2dxdy+\lambda_2\int_{outside(\Gamma)}|z(x,y)-c_2|^2dxdy$ to the model (2.2) where $\lambda_1,\lambda_2$ are any constants and $c_1,c_2$ are average values of the given image $z(x,y)$ inside and outside $\Gamma$. Thus we propose the following model

$$\min_{\phi(x,y),c_1,c_2} F(\phi(x,y),c_1,c_2), \tag{3.1}$$

with

$$\begin{aligned} F(\Gamma,c_1,c_2)=\mu\int_\Gamma dg(|\nabla z(x,y)|)ds+\lambda_1\int_{inside(\Gamma)}|z(x,y)-c_1|^2dxdy \\ +\lambda_2\int_{outside(\Gamma)}|z(x,y)-c_2|^2dxdy, \end{aligned} \tag{3.2}$$

where $\mu$ is a positive parameter. Clearly if $\lambda_1=\lambda_2=0$ this minimization problem reduces to minimization problem (2.2).

Thus we consider the following minimization problem

$$\min_{\phi(x,y),c_1,c_2} F(\phi(x,y),c_1,c_2). \tag{3.3}$$

using the level set formulation of (3.2)

$$\begin{aligned} F(\phi(x,y),c_1,c_2)=\mu\int_\Omega d(x,y)g(|\nabla z(x,y)|)|\nabla H(\phi(x,y))|dxdy \\ +\lambda_1\int_\Omega|z(x,y)-c_1|^2H(\phi(x,y))dxdy \\ +\lambda_2\int_\Omega|z(x,y)-c_2|^2(1-H(\phi(x,y)))dxdy, \end{aligned} \tag{3.4}$$

where $H$ is again the Heaviside function. Further using the regularized Heaviside function $H_\epsilon$, we consider the following minimization problem

$$\min_{\phi(x,y),c_1,c_2} F_\epsilon(\phi(x,y),c_1,c_2), \tag{3.5}$$

where

$$\begin{aligned} F_\epsilon(\phi(x,y),c_1,c_2)=\mu\int_\Omega d(x,y)g(|\nabla z(x,y)|)\delta_\epsilon(\phi(x,y))|\nabla\phi(x,y)|dxdy \\ +\lambda_1\int_\Omega|z(x,y)-c_1|^2H_\epsilon(\phi(x,y))dxdy \\ +\lambda_2\int_\Omega|z(x,y)-c_2|^2(1-H_\epsilon(\phi(x,y)))dxdy. \end{aligned} \tag{3.6}$$

Keeping $\phi(x,y)$ fixed and minimizing with respect to $c_1$ and $c_2$ we have the following equations for computing $c_1$ and $c_2$:

$$c_1(\phi(x,y)) = \frac{\int_\Omega z(x,y)H_\epsilon(\phi(x,y))dxdy}{\int_\Omega H_\epsilon(\phi(x,y))dxdy} \tag{3.7}$$

if $\int_\Omega H_\epsilon(\phi(x,y))dxdy > 0$ (i.e. if the curve has a nonempty interior in $\Omega$), and

$$c_2(\phi(x,y)) = \frac{\int_\Omega z(x,y)(1-H_\epsilon(\phi(x,y)))dxdy}{\int_\Omega (1-H_\epsilon(\phi(x,y)))dxdy} \tag{3.8}$$

if $\int_\Omega (1-H_\epsilon(\phi(x,y)))dxdy > 0$ (i.e. if the curve has a nonempty exterior in $\Omega$).

Now keeping $c_1$ and $c_2$ fixed, we minimize (3.6) with respect to $\phi(x,y)$. To minimize $F_\epsilon$ we use the Gâteaux derivatives of the functional $F_\epsilon$

$$\lim_{h\to 0}\frac{1}{h}\Big(F_\epsilon(\phi+h\psi,c_1,c_2)-F_\epsilon(\phi,c_1,c_1)\Big)=0,$$

which leads to

$$\begin{aligned}\mu\int_\Omega \mu d(x,y)g(|\nabla z(x,y)|)\left(\delta'_\epsilon(\phi)|\nabla\phi|\psi+\delta_\epsilon(\phi)\frac{\nabla\phi\cdot\nabla\psi}{|\nabla\phi|}\right)dxdy\\ +\int_\Omega \delta_\epsilon(\phi)(\lambda_1(z(x,y)-c_1)^2-\lambda_2(z(x,y)-c_2)^2)\psi dxdy=0,\end{aligned} \tag{3.9}$$

where $\psi$ is a test function of the same type as $\phi$. From Green's Theorem we have

$$\int_\Omega v\nabla.\vec{w}dx = -\int_\Omega \nabla v.\vec{w}dx+\int_{\partial\Omega} v\vec{w}.\vec{n}ds, \tag{3.10}$$

where $\vec{n}$ is the unit normal vector to the boundary of $\Omega$. Hence taking

$$\psi = v, \quad G(x,y)\frac{\delta_\epsilon(\phi)}{|\nabla\phi|}\nabla\phi=\vec{w},$$

we obtain

$$\begin{aligned}&\int_\Omega \psi\nabla\cdot\Big(G(x,y)\frac{\delta_\epsilon(\phi)}{|\nabla\phi|}\nabla\phi\Big)dx\\ =&-\int_\Omega \nabla\psi\cdot G(x,y)\frac{\delta_\epsilon(\phi)}{|\nabla\phi|}\nabla\phi dx+\int_{\partial\Omega}\psi G(x,y)\frac{\delta_\epsilon(\phi)}{|\nabla\phi|}\nabla\phi\cdot\vec{n}ds,\end{aligned}$$

i.e.,

$$\begin{aligned}&\int_\Omega G(x,y)\delta_\epsilon(\phi)\frac{\nabla\phi\cdot\nabla\psi}{|\nabla\phi|}dx\\ =&-\int_\Omega \psi\nabla\cdot\left(G(x,y)\frac{\delta_\epsilon(\phi)}{|\nabla\phi|}\nabla\phi\right)dx+\int_{\partial\Omega}\psi G(x,y)\frac{\delta_\epsilon(\phi)}{|\nabla\phi|}\frac{\partial\phi}{\partial\vec{n}}ds,\end{aligned}$$

where

$$\nabla\phi\cdot\vec{n}=\frac{\partial\phi}{\partial\vec{n}},\quad G(x,y)=d(x,y)g(|\nabla z(x,y)|).$$

Thus Eq. (3.9) becomes

$$\begin{aligned}&\int_\Omega \mu G(x,y)\delta_\epsilon'(\phi)|\nabla\phi|\psi dxdy+\int_{\partial\Omega}\mu G(x,y)\frac{\delta_\epsilon(\phi)}{|\nabla\phi|}\frac{\partial\phi}{\partial\vec{n}}\psi ds\\&\quad-\int_\Omega\mu\delta_\epsilon(\phi)\nabla\cdot\left(G(x,y)\frac{\nabla\phi}{|\nabla\phi|}\right)\psi dxdy-\int_\Omega\mu\delta_\epsilon'(\phi)G(x,y)\nabla\phi\cdot\frac{\nabla\phi}{|\nabla\phi|}\psi dxdy\\&\quad+\int_\Omega\delta_\epsilon(\phi)(\lambda_1(z(x,y)-c_1)^2-\lambda_2(z(x,y)-c_2)^2)\psi dxdy=0.\end{aligned}$$

Further the following form holds

$$\begin{aligned}&-\int_\Omega\mu\delta_\epsilon(\phi)\nabla\cdot\left(G(x,y)\frac{\nabla\phi}{|\nabla\phi|}\right)\psi dxdy+\int_{\partial\Omega}\mu G(x,y)\frac{\delta_\epsilon(\phi)}{|\nabla\phi|}\frac{\partial\phi}{\partial\vec{n}}\psi ds\\&\quad+\int_\Omega\delta_\epsilon(\phi)(\lambda_1(z(x,y)-c_1)^2-\lambda_2(z(x,y)-c_2)^2)\psi dxdy=0,\end{aligned}$$

for all test functions $\psi$. Hence we have the following Euler-Lagrange equation for $\phi$:

$$\begin{aligned}&\delta_\epsilon(\phi)\mu\nabla\cdot\left(G(x,y)\frac{\nabla\phi}{|\nabla\phi|}\right)-\delta_\epsilon(\phi)\left(\lambda_1(z(x,y)-c_1)^2-\lambda_2(z(x,y)-c_2)^2\right)=0,\\&G(x,y)\frac{\delta_\epsilon(\phi)}{|\nabla\phi|}\frac{\partial\phi}{\partial\vec{n}}=0,\quad\text{on }\partial\Omega.\end{aligned}\tag{3.11}$$

The above PDE may be considered as the steady state form of the following evolution equation

$$\begin{cases}\dfrac{\partial\phi}{\partial t}=\mu\delta_\epsilon(\phi(x,y))\nabla\cdot\left(G(x,y)\dfrac{\nabla\phi}{|\nabla\phi|}\right)\\\qquad\qquad-\delta_\epsilon(\phi)\left(\lambda_1(z(x,y)-c_1)^2-\lambda_2(z(x,y)-c_2)^2\right),\\G(x,y)\dfrac{\delta_\epsilon(\phi)}{|\nabla\phi|}\dfrac{\partial\phi}{\partial n}\Big|_{\partial\Omega}=0,\end{cases}\tag{3.12}$$

with $\phi(x,y,0)=\phi_0(x,y)$.

To prevent the curve from stopping on a non-significant local minimum and to initialize the iteration process with a curve inside the object to be detected [16,18], a balloon term $\alpha G(x,y)|\nabla\phi|$ is now added to speed up the convergence of the evolution equation as done in M-1, where $\alpha$ is a constant. Thus Eq. (3.12) with the balloon term can be written

as

$$\begin{cases} \dfrac{\partial\phi}{\partial t}=\mu\delta_\epsilon(\phi(x,y))\nabla\cdot\Big(G(x,y)\dfrac{\nabla\phi}{|\nabla\phi|}\Big) \\ \qquad -\delta_\epsilon(\phi)\Big(\lambda_1(z(x,y)-c_1)^2-\lambda_2(z(x,y)-c_2)^2\Big)+\alpha G(x,y)|\nabla\phi|, \\ G(x,y)\dfrac{\delta_\epsilon(\phi)}{|\nabla\phi|}\dfrac{\partial\phi}{\partial n}\Big|_{\partial\Omega}=0, \end{cases} \tag{3.13}$$

with $\phi(x,y,0)=\phi_0(x,y)$. Existence and uniqueness of the solution can be proved along similar lines to [18].

# 4 Numerical methods

We now present two numerical methods for solving the nonlinear parabolic PDE (3.13).

## 4.1 Semi-implicit method

First write the PDE (3.13) as

$$\frac{\partial\phi}{\partial t}=\mu\delta_\epsilon(\phi(x,y))\left[G(x,y)\nabla\cdot\Big(\frac{\nabla\phi}{|\nabla\phi|}\Big)+\nabla G(x,y)\cdot\left(\frac{\nabla\phi}{|\nabla\phi|}\right)\right]+f(x,y),$$

where

$$f(x,y)=\delta_\epsilon(\phi)\Big(-\lambda_1(z-c_1)^2+\lambda_2(z-c_2)^2\Big)+\alpha G(x,y)|\nabla\phi|.$$

Using the differences $\triangle_+^x,\triangle_-^x,\cdots$ given by,

$$\begin{aligned} &\triangle_-^x\phi_{i,j}=\phi_{i,j}-\phi_{i-1,j}, \quad \triangle_+^x=\phi_{i+1,j}-\phi_{i,j}, \\ &\triangle_-^y\phi_{i,j}=\phi_{i,j}-\phi_{i,j-1}, \quad \triangle_+^y=\phi_{i,j+1}-\phi_{i,j}, \end{aligned} \tag{4.1}$$

and a semi-implicit scheme, the discretized form of equation (4.1) is:

$$\begin{aligned} \frac{\phi_{i,j}^{k+1}-\phi_{i,j}^k}{\triangle t}=\mu\delta_\epsilon(\phi_{i,j}^k)G_{i,j}\Bigg[&\frac{1}{h_1^2}\triangle_-^x\left(\frac{\triangle_+^x\phi_{i,j}^{k+1}}{\sqrt{(\triangle_+^x\phi_{i,j}^k/h_1)^2+(\triangle_+^y\phi_{i,j}^k/h_2)^2}}\right) \\ &+\frac{1}{h_2^2}\triangle_-^y\left(\frac{\triangle_+^y\phi_{i,j}^{k+1}}{\sqrt{(\triangle_+^x\phi_{i,j}^k/h_1)^2+(\triangle_+^y\phi_{i,j}^k/h_2)^2}}\right)\Bigg] \\ &+\mu\frac{\delta_\epsilon(\phi_{i,j}^k)}{|\nabla\phi_{i,j}^k|}\left\{\frac{1}{h_1^2}\triangle_+^xG(x,y)\triangle_+^x\phi_{i,j}^{k+1}+\frac{1}{h_2^2}\triangle_+^yG(x,y)\triangle_+^y\phi_{i,j}^{k+1}\right\}+f_{i,j}. \end{aligned}$$

We usually use $h_1=h_2=1$, so we have

$$\frac{\phi_{i,j}^{k+1}-\phi_{i,j}^{k}}{\triangle t}=\mu\delta_\epsilon(\phi_{i,j}^k)G_{i,j}\Big[(\phi_{i+1,j}^{k+1}-\phi_{i,j}^{k+1})D_{i,j}-(\phi_{i,j}^{k+1}-\phi_{i-1,j}^{k+1})D_{i-1,j}$$
$$+(\phi_{i,j+1}^{k+1}-\phi_{i,j}^{k+1})D_{i,j}-(\phi_{i,j}^{k+1}-\phi_{i,j-1}^{k+1})D_{i,j-1}\Big]+f_{i,j}$$
$$+\mu\frac{\delta_\epsilon(\phi_{i,j}^k)}{|\nabla\phi_{i,j}^k|}\Big\{\triangle_+^x G(x,y)(\phi_{i+1,j}^{k+1}-\phi_{i,j}^{k+1})+\triangle_+^y G(x,y)(\phi_{i,j+1}^{k+1}-\phi_{i,j}^{k+1})\Big\}, \quad (4.2)$$

if we denote by

$$D_{i-1,j}=1/\sqrt{(\triangle_+^x\phi_{i-1,j}^k)^2+(\triangle_+^y\phi_{i-1,j}^k)^2}, \quad D_{i,j}=1/\sqrt{(\triangle_+^x\phi_{i,j}^k)^2+(\triangle_+^y\phi_{i,j}^k)^2},$$
$$D_{i,j-1}=1/\sqrt{(\triangle_+^x\phi_{i,j-1}^k)^2+(\triangle_+^y\phi_{i,j-1}^k)^2}. \quad (4.3)$$

As the coefficients $D_{i-1,j}$, $D_{i,j}$ and $D_{i,j-1}$ has been freezed at $k$, Eq. (4.2) gives a linear system of equations which can be solved by an iterative method. The semi-implicit method can allow large time steps but the main drawback is the computational cost of the associated linear systems [33] for large images. Hence we shall develop an AOS method as done in [23,32] to solve the PDE (3.13) which will be our preferred method for M-2.

### 4.2 An additive operator splitting method

Consider Eq. (3.13) in the form

$$\frac{\partial\phi}{\partial t}=\mu\delta_\epsilon(\phi)\nabla\cdot(F\nabla\phi)+f=\mu\delta_\epsilon(\phi)\Big(\partial_x(F\partial_x\phi)+\partial_y(F\partial_y\phi)\Big)+f, \quad (4.4)$$

where

$$f=-\delta_\epsilon(\phi)(\lambda_1(z-c_1)^2-\lambda_2(z-c_2)^2)+\alpha G(x,y)|\nabla\phi|, \quad F=\frac{G}{|\nabla\phi|}.$$

The AOS scheme [23,32] splits the $m$-dimensional spatial operator into a sum of $m$ one-dimensional space discretizations. Therefore we consider the first of two one-dimensional problems

$$\frac{\phi_i^{k+1}-\phi_i^k}{\triangle t}=\mu\delta_\epsilon(\phi)\left((\frac{F_i^k+F_{i+1}^k}{2})(\phi_{i+1}^{k+1}-\phi_i^{k+1})-(\frac{F_i^k+F_{i-1}^k}{2})(\phi_i^{k+1}-\phi_{i-1}^{k+1})\right)+f_i, \quad (4.5)$$

i.e.,

$$\phi_i^{k+1}=\phi_i^k+\mu\triangle t(c_1\phi_{i+1}^{k+1}-c_2\phi_i^{k+1}+c_3\phi_{i-1}^{k+1})+f_i, \quad (4.6)$$

where

$$c_1=\delta_\epsilon(\phi)\frac{F_i^k+F_{i+1}^k}{2},\quad c_2=\delta_\epsilon(\phi)\frac{F_{i-1}^k+2F_i^k+F_{i+1}^k}{2},\quad c_3=\delta_\epsilon(\phi)\frac{F_i^k+F_{i-1}^k}{2}.$$

After we solve the system of equations (4.6) in the $x$-direction, we then solve a similar system in the $y$-direction before averaging the two solutions. In matrix notation the process can be written as

$$(I-2\triangle tA_l(\phi^k))\phi_l^{k+1}=f^k,\quad \text{for } l=1,2,$$

and

$$\phi^{k+1}=\frac{1}{2}\sum_{l=1}^{2}\phi_l^{k+1},$$

where $I$ is the identity matrix and $A_l$ for $l=1,2$ are tridiagonal matrices derived from (4.6).

# 5 Experimental results

In this section we present some simulation results illustrating the old method M-1 and the new method M-2. We shall observe that M-2 is better in terms of robustness, quality and speed.

Firstly we present some simple examples when M-1 does not work well. Secondly we show that our model M-2 works fine on these examples and we also test our model on real images. Lastly we give evidence that our model M-2 is faster than M-1 in convergence in terms of number of iterations (and CPU time as the complexity per iteration of both model is similar).

## 5.1 Performance of M-1

The performance of M-1 is strongly influenced by the initial contour. When it is selected to be close to the final solution, the result of M-1 is very good as shown in Fig. 1 where the left plot shows the initial circle chosen to be quite close to the final contour of the rectangle which is segmented on the right plot correctly by M-1. In a simple test, M-1 is found not to converge properly if the radius of the initial contour is halved (in comparison M-2 would work for either initial contour). The same observation has been made on other test images; in Fig. 2 we show similar initial contour and segmented results for a realistic CT image – here again starting from a smaller circle would fail M-1 (but not M-2).

Heavy noise in a given image can also affect the quality of segmentation by M-1, even if the initial contour is chosen quite close. In Fig. 3, we show such an example of a synthetic noisy image to detect the rectangle in it with 4 markers shown in the figure in red dots. M-1 clearly fails to detect the rectangle when the initial contour is quite close. There, the left figure is the original image with initial data (red dots are the markers), the middle is the result after 1000 iterations (hardly any improvement) and the far right is the

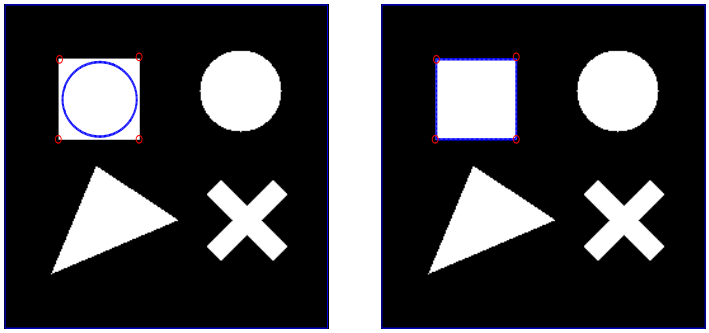

(a) Original with initial data (b) after 1000 iterations

Figure 1: M-1 results I: successful detection of the rectangle in a synthetic clean image with 4 markers and the initial guess (left plot) quite close the final solution (right plot).

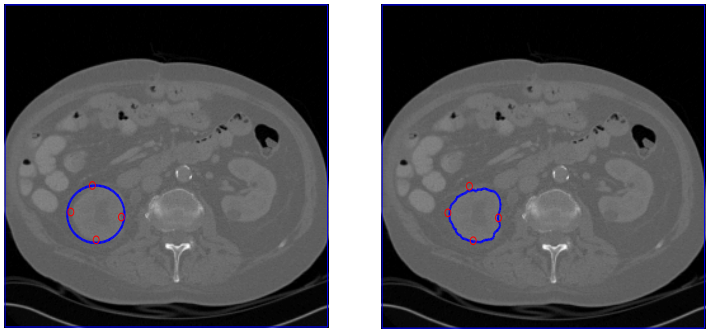

(a) Original with initial data (b) after 1000 iterations

Figure 2: M-1 results II: successful detection of the rectangle in a real CT image with 4 markers and the initial guess (left plot) quite close the final solution (right plot).

final result after 20000 iterations where the level set function $\phi$ does not move any more. Here the parameters used are: $\phi_0=\sqrt{(x-x_0)^2+(y-y_0)^2}-25$ where

$$x_0=\frac{\sum x\text{-comp of markers}}{\text{no. of markers}},\quad y_0=\frac{\sum y\text{-comp of markers}}{\text{no. of markers}},$$

and $\sigma=4$, $\alpha=-0.00151$, $\triangle t=1$. To improve the result, in Fig. 4, M-1 is tested on the same image, where the image is filtered first. The initial condition is $\phi_0=\sqrt{(x-x_0)^2+(x-y_0)^2}-25$, where $x_0$,$y_0$ are the averages of $x$,$y$-components of the markers. We show on the plot the original image with initial contour, the result after 800 iterations in the middle plot and the result after 16000 iterations on the right. Clearly the final result is not satisfactory. Here filtering can improve on segmentation by M-1 but excessive filtering (smoothing) can smear edges (as seen in Fig. 4).

In Fig. 5, M-1 is tested on an artificial image. Here with only partial success, it only detects the outer boundary of the letter O using the parameters are $\mu=(\text{size of } z)^2/1400$,

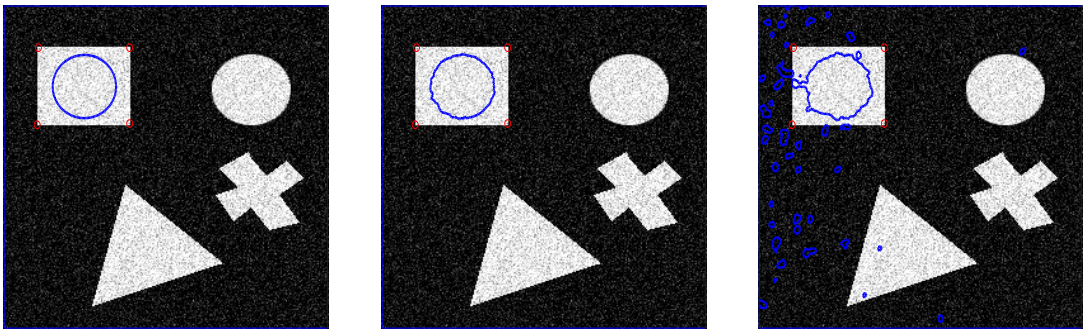

(a) Original with initial data (b) after 1000 iterations (c) after 20000 iterations

Figure 3: M-1 results: unsuccessful detection of the rectangle in a synthetic noisy image with 4 markers and initial guess $\phi_0=\sqrt{(x-x_0)^2+(x-y_0)^2}-25$, where $x_0,y_0$ are the averages of $x,y$-components of the markers, $\alpha=-0.00151$ and $\sigma=4$.

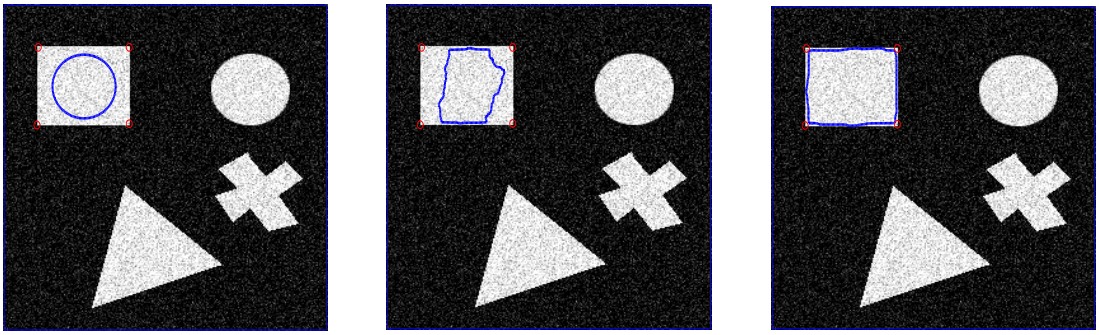

(a) Original with initial data (b) after 800 iterations (c) after 16000 iterations

Figure 4: M-1 results: partially successful detection of the rectangle in a synthetic noisy image with 4 markers ideally placed. Here the initial guess $\phi_0=\sqrt{(x-x_0)^2+(x-y_0)^2}-25$, where $x_0,y_0$ are the averages of $x,y$-components of the markers, $\alpha=-0.0011$ and $\sigma=4$.

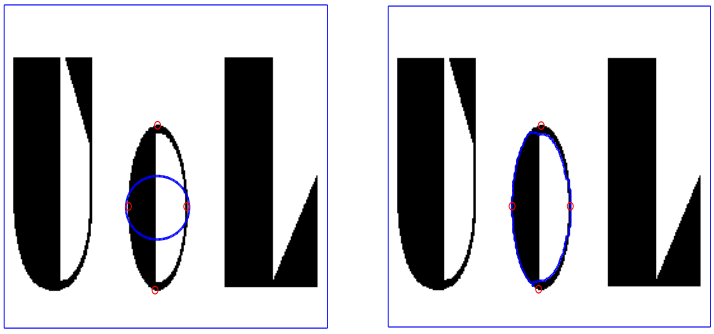

(a) Original with initial data (b) after 900 iterations

Figure 5: M-1 results: partially successful detection of the letter O in the UOL image as the inner boundary of the letter O is left out.

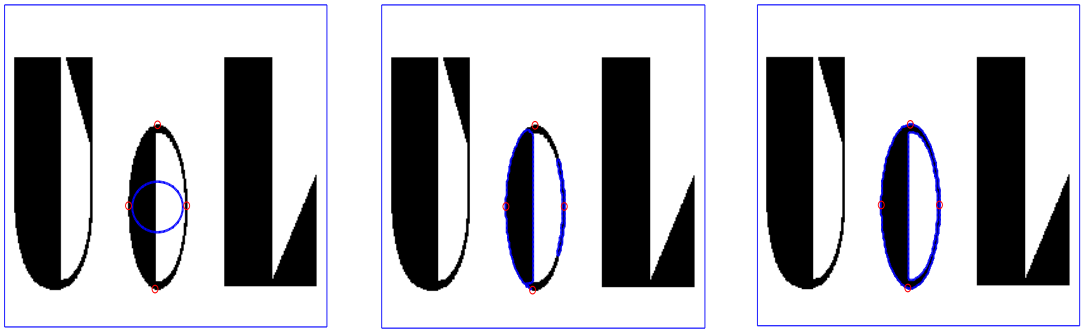

(a) Original with initial data (b) after 35 iterations (c) after 250 iterations

Figure 6: M-2 results: successful detection of the letter O in the image UOL with 4 markers placed in ideal positions and with initial guess $\phi_0$ as in Fig. 5. $\mu=(\text{size of } z)^2/1400$, $\lambda_1=0.00951$, $\lambda_2=0.0095$, $\alpha=-5.1\times10^{-4}$ and $\sigma=4$.

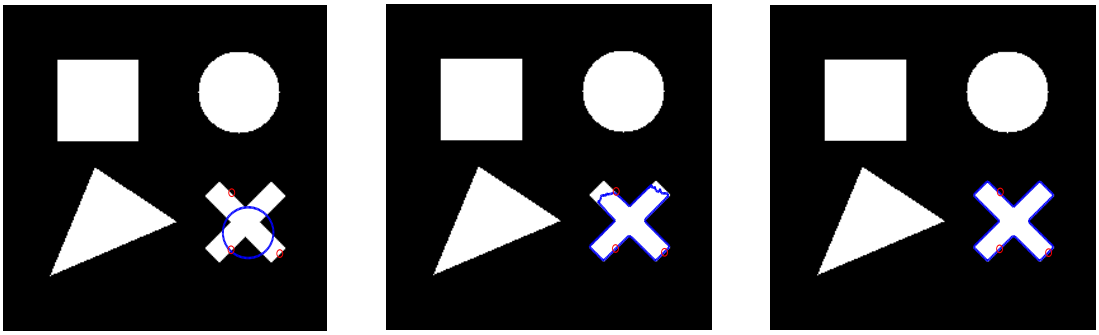

(a) Original with initial data (b) after 4 iterations (c) after 14 iterations

Figure 7: M-2 results: successful detection of the object X in a clean and synthetic image with 3 markers. Here $\mu=100$, $\alpha=-0.001$, $\lambda_1=0.1$, $\lambda_2=0.1$ and $\sigma=4$.

$\lambda_1=0.00951$, $\lambda_2=0.0095$, $\alpha=-5.1\times10^{-4}$ and $\sigma=4$. To see a successful segmentation in this case, the initial contour must be further modified to be close to the solution. And here and from now on, $\phi_0=\sqrt{(x-x_0)^2+(y-y_0)^2}-r_0$, $x_0$,$y_0$ are the averages of the $x$,$y$-components of the markers and $r_0=\min_{\mathbf{y}}\|\mathbf{x}-\mathbf{y}\|$ where $\mathbf{x}=(x_0,y_0)$ and $\mathbf{y}\in A$.

## 5.2 Improved performance of M-2

In Fig. 6, M-2 is tested on the artificial image of Fig. 5, using the same parameters, where M-1 did not do very well. We set the initial condition as above in Fig. 5. In particular, $\phi_0=\sqrt{(x-x_0)^2+(x-y_0)^2}-r_0$ where $x_0$,$y_0$ are defined as above and $r_0=\min_{\mathbf{y}}\|\mathbf{x}-\mathbf{y}\|$ where $\mathbf{x}=(x_0,y_0)$ and $\mathbf{y}\in A$. Clearly the object is segmented successfully.

In Fig. 7 our model M-2 is tested on an artificial image to detect the object X with 3 markers. The object X is segmented successfully.

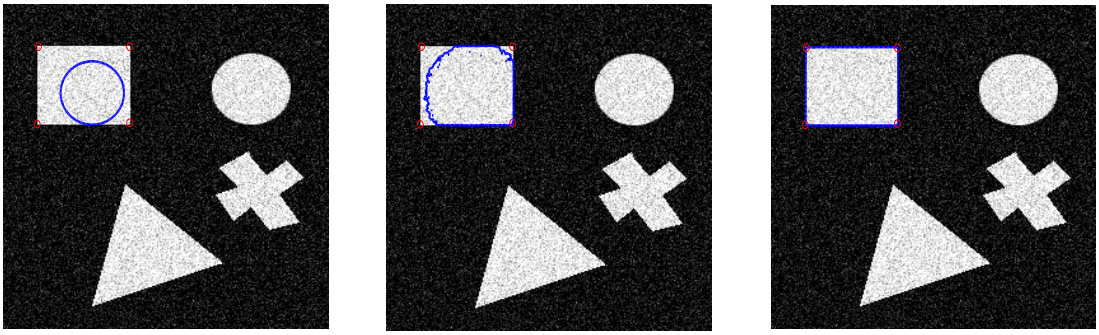

(a) Original with initial data (b) after 15 iterations (c) after 130 iterations

Figure 8: M-2 results: successful detection of the rectangle in a noisy synthetic image with 4 markers with initial guess set similarly to before and other parameters the same as in Fig. 7.

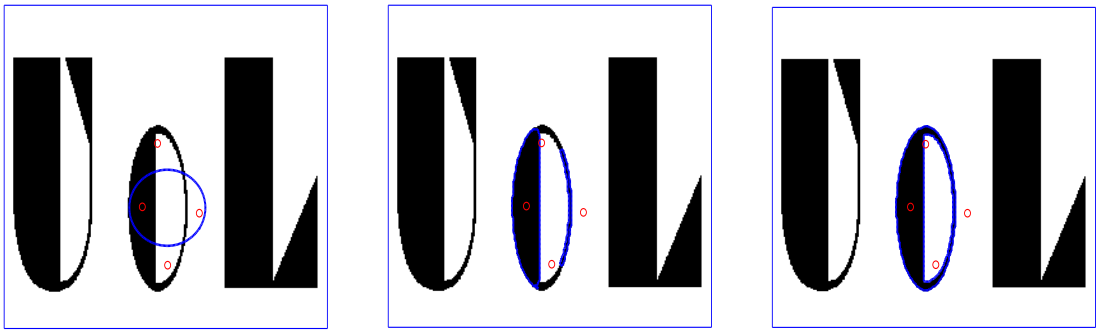

(a) Original with initial data (b) after 35 iterations (c) after 250 iterations

Figure 9: M-2 results: successful detection of the letter O in the image UOL with 4 markers placed away from the boundaries. The same parameters as in Fig. 6 are used.

In Fig. 8, M-2 is tested on synthetic noisy image with 4 markers and parameters $\mu=100$, $\alpha=-0.001$, $\lambda_1=0.1$, $\lambda_2=0.1$ and $\sigma=4$. The left plot is the original image with initial data and the middle is the result after 15 iterations. Again the required object (shown on the right plot) is successfully detected.

In Fig. 9, it is shown that if the markers are not exactly on boundary, the object can be detected. The same data are used as in Fig. 6.

In Fig. 10, we show results where M-1, M-2 fail to segment the image if the initial guess $\phi_0$ is far from the markers (away from the object to be detected).

In Fig. 11 our model is tested on a real brain MRI image to detect a tumor with 4 markers. The other parameters used are $\mu=(\text{size of } z)^2/1000$, $\lambda_1=0.001$, $\lambda_2=0.001$, $\alpha=-1.51\times10^{-3}$ and $\sigma=4$. The correct segmentation is obtained after 200 iterations.

In Fig. 12, we test the model on real knee MRI image with 3 markers (also work with 2 markers) and the following parameters $\mu=(\text{size of } z)^2/10$, $\lambda_1=\lambda_2=0.000051$, $\alpha=-1.51\times10^{-3}$ and $\sigma=4$. The correct segmentation is obtained after 120 iterations as

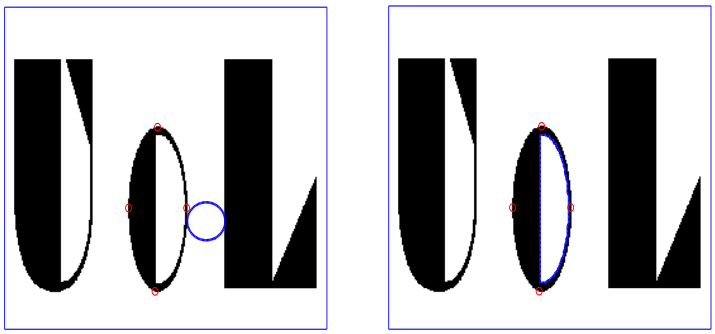

Figure 10: M-1 and M-2 results: unsuccessful detection of the letter O in the image UOL with 4 markers placed away from the boundaries and with a (wrong) initial guess $\phi_0$ 'outside' the markers (usually it should be inside).

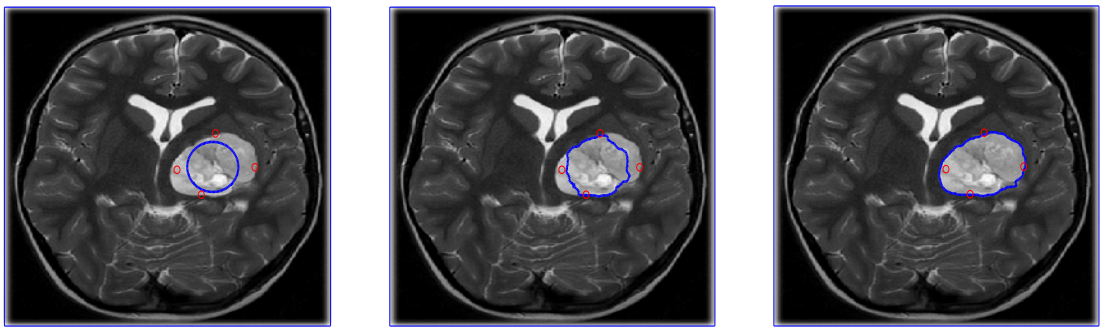

(a) Original with initial data (b) after 10 iterations (c) after 200 iterations

Figure 11: M-2 results: correct detection of tumor region in a real brain MRI image with 4 markers. $\mu = (\text{size of } z)^2/1000$, $\lambda_1 = 0.001$, $\lambda_2 = 0.001$, $\alpha = -1.51\times10^{-3}$ and $\sigma = 4$.

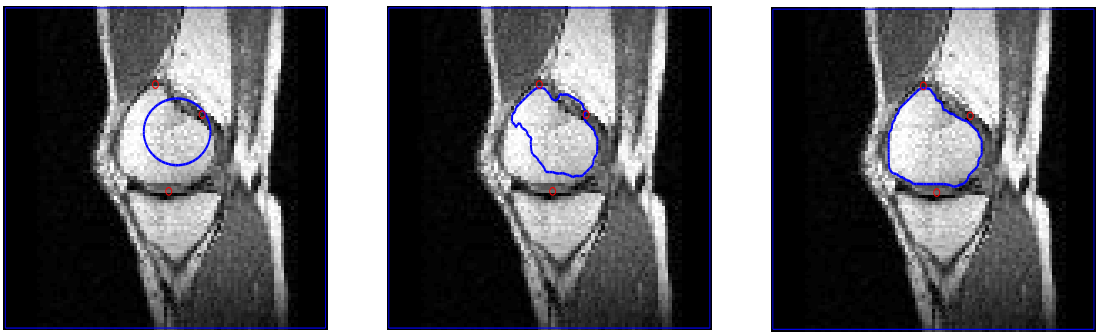

(a) Original with initial data (b) after 20 iterations (c) after 170 iterations

Figure 12: M-2 results: correct detection of the knee in a real knee MRI image with 3 markers.

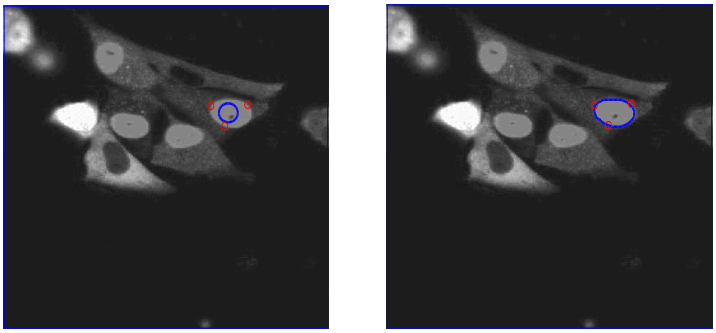

(a) Original with initial data (b) after 100 iterations

Figure 13: Further M-2 results I: successful detection of a special region (right plot) in a cell image with 3 markers and the initial guess as on the left plot.

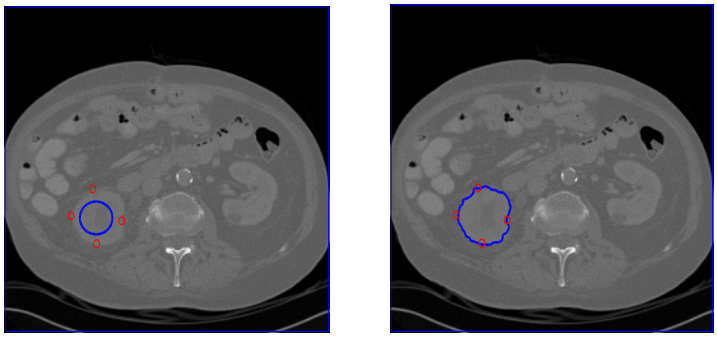

(a) Original with initial data (b) after 120 iterations

Figure 14: Further M-2 results II: successful detection of a special (right plot) in a real CT image with 4 markers and the initial guess as on the left plot.

shown on the right plot.

Finally in Figs. 13 and 14, we show the correctly segmented results of two further real images (right plots) by M-2, starting from the initial contours (left plots). We remark that the same results can be obtained by M-1, *only* if the initial contours are enlarged to be as close as to the final solutions (although M-1 cannot work with the initial contours of Figs. 13 and 14).

### 5.3 Speed comparison of M-1 and M-2

Lastly, we compare results of M-1 and M-2 by number of iterations as each iteration of either method, of AOS type, has a comparable complexity. In Fig. 15, the successful segmentation of a disc in an artificial image is obtained in 500 iterations by M-1. The same test is repeated in Fig. 16 using our new model M-2 obtaining a comparable result in only 100 iterations. Similar comparison results have been observed in many other experiments

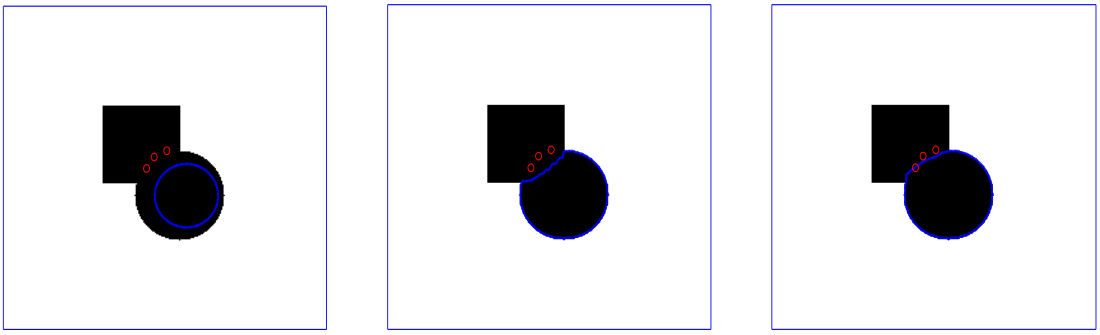

(a) Original with initial data (b) after 100 iterations (c) after 500 iterations

Figure 15: Slower convergence of M-1 to detect the disc in the disc-rectangle image using 3 markers with initial guess as shown.

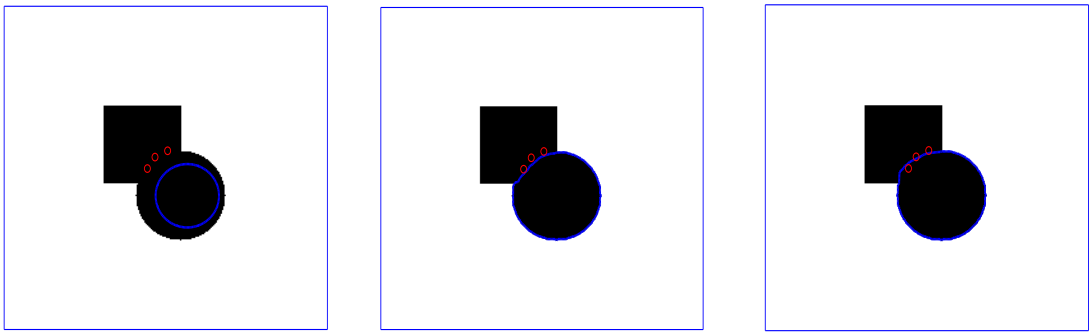

(a) Original with initial data (b) after 15 iterations (c) after 100 iterations

Figure 16: Faster convergence of M-2 to detect the same disc as in Fig. 15 using 3 markers. Clearly M-2 (100 steps) is faster than M-1 (500 steps) to reach the similar quality.

and clearly M-2 converges faster. Further development of even faster solvers [4, 9] for both methods will be carried out in the near future.

## 6 Conclusions

In this paper we proposed a new variational model for selective image segmentation based on geodesic active contours and the Chan-Vese model. Our new model (without using Gaussian filter) is particularly good for noisy images. From testing the new model on real images, we observe that it is also faster than the existing model in term of number of iterations. The new model works even if the markers are not on the desired boundary as long as the initial contour is contained within the markers, as shown by the numerical experiments.

**References**

[1] R. Adams and L. Bischof, Seeded region growing. IEEE Trans. Pattern Analysis and Machine Intelligence, 16(6):641-647, 1994.
[2] L. Alvarez, P.-L. Lions and J. M. Morel, Image selective smoothing and edge detection by nonlinear diffusion. SIAM J. Numer. Anal., 29(3): 845–866, 1992.
[3] G. Aubert and L. Vese, A variational method in image recovery. SIAM J. Numer. Anal., 34: 1948–1979, 1997.
[4] N. Badshah and K. Chen, Multigrid method for the Chan-Vese model in variational segmentation. Commu. Comput. Phys., 4(2):294-316, 2008.
[5] N. Badshah and K. Chen, On two multigrid algorithms for modelling variational multiphase image segmentation. IEEE Trans. Image Proc., 18(5):1097-1106, 2009.
[6] N. Badshah and K. Chen, An optimization-based multilevel method for variational image segmentation models. Submitted, 2009.
[7] X. Bresson, S. Esedoglu, P. Vandergheynst, J.P. Thiran, and S. Osher. Global minimizers of the active contour/snake model. J. Math. Imaging and Vision, 28(2):151-167, 2007.
[8] V. Caselles, R. Kimmel and G. Sapiro. Geodesic active contours. Int. J. Computer Vision, 22(1):61-79, 1997.
[9] T. F. Chan and K. Chen. An optimization-based multilevel algorithm for total variation image denoising, SIAM J. Multiscale Mod. Simu., 5(2):615-645, 2006.
[10] T. F. Chan, K. Chen and X. C. Tai, Nonlinear multilevel schemes for solving the total variation image minimization problem, In: "Image Processing Based on PDEs", eds. X.-C. Tai, K.-A. Lie, T.F. Chan and S. Osher, pp.69-94, Springer-Verlag, 2006.
[11] T. F. Chan, S. Esedolgu and M. Nikolova, Algorithm for finding global minmizers of image segmentation and denoising models. SIAM J. Appl. Math., 66:1632-1648, 2006.
[12] T. F. Chan and J. H. Shen, Image Processing and Analysis - Variational, PDE, wavelet, and stochastic methods, SIAM Publications, Philadelphia, USA, 2005.
[13] T. F. Chan and L. A. Vese. An efficient variational multiphase motion for the Mumford-Shah segmentation model. IEEE Asilomar Conference on Signals Systems and Computers, 1:490-494, 2000.
[14] T. F. Chan and L. A. Vese. Active contours without edges. IEEE Transactions on Image Processing, 10(2):266-277, 2001.
[15] Ke Chen. Matrix Preconditioning Techniques and Applications. Cambridge University Press, Cambridge, UK, 2005.
[16] D. Cohen. On active contour models and ballons. CVGIP: Image Understanding, 53:211-218, 1991.
[17] C. Gout, C. Le Guyader and L. A. Vese. Segmentation under geometrical consitions with geodesic active contour and interpolation using level set methods. Numerical Algorithms, 39:155-173, 2005.
[18] C. Le Guyader and C. Gout. Geodesic active contour under geometrical conditions theory and 3D applications. Numerical Algorithms, 48:105-133, 2008.
[19] M. Jeon, M. Alexander, W. Pedrycz and N. Pizzi, Unsupervised hierarchical image segmentation with level set and additive operator splitting. Pattern Recognition Letters, 26:1461-1469, 2005.
[20] M. Kass, A. Witkin, and D. Terzopoulos. Snakes: Active contour models. International Journal of Computer Vision, 1(4):321-331, 1987.
[21] Y. Leclerc, Region growing using the MDL principle, In: DAPPRA Image Understanding

Workshop, 1990.
[22] D. Mumford and J. Shah. Optimal approximation by piecewise smooth functions and associated variational problems. Communications on Pure Applied Mathematics, 42:577-685, 1989.
[23] T. Lu, P. Neittaanmäki, and X.-C. Tai. A parallel splitting up method and its application to Navier-Stokes equations. Appl. Math. Lett., 4(2):25-29, 1991.
[24] J.-M. Morel and S. Solimini, Variational methods in image segmentation, Vol.14, Progress in Nonlinear Differential Equations and Their Applications. Birkhäuser, Boston, 1995.
[25] S. Osher and R. Fedkiw, Level Set Methods and Dynamic Implicit Surfaces. Springer, New York, 2003.
[26] S. Osher and J. A. Sethian. Fronts propagating with curvature-dependent speed: algorithms based on Hamilton-Jacobi formulations. J. Comput. Phys., 79(1):12-49, 1988.
[27] L. I. Rudin, S. Osher and E. Fatemi, Nonlinear total variation based noise removal algorithms, Physica D, 60:259-268, 1992.
[28] J. A. Sethian, Level Set Methods and Fast Marching Methods: Evolving interfaces in computational Geometry, Fluid Mechanics, Computer Vision, and Materials Sciences. Cambridge University Press, 2002.
[29] W. B. Tao and Xue-Cheng Tai, Multiple piecewise constant active contours for image segmentation using graph cuts optimization, UCLA CAM report 09-13, 2009.
[30] L. A. Vese and T. F. Chan, A multiphase level set framework for image segmentation using the Mumford and Shah model, Comm. Pure Appl. Math., 50(3):271-293, 2002.
[31] L. Vincent and Soille, Watersheds in Digital Spaces - an efficient algorithm based on immersion. IEEE Trans. Pattern Analysis and Machine Learning, 6:583-598, 1994.
[32] J. Weickert, B. M. ter Haar Romeny and M. A. Viergever, Efficient and reliable schemes for nonlinear diffusion filtering, IEEE Trans. Image Proc., 7:398-410, 1998.
[33] J. Weickert and G. Kühne, Fast methods for implicit active contours models. In: Geometric Level Set Methods in Imaging, Vision, and Graphics, pp.43-58, eds. S. Osher and N. Paragios, Springer, 2003.
[34] H. K. Zhao, S. Osher, B. Merriman and M. Kang, Implicit and non-parametric shape reconstruction from unorganized data using a variational level set method. Computer Vision and Image Understanding., 80(3):295-314, 2000.